

**FRBs: the Dispersion Measure of Host Galaxies**

M. Jaroszynski

Astronomical Observatory, University of Warsaw, Al. Ujazdowskie 4, 00-478 Warszawa,  
Poland

## ABSTRACT

Using the results of the IllustrisTNG simulation we estimate the dispersion measure which may be attributed to halos of so called host galaxies of fast radio bursts sources (FRBs). Our results show that in contradiction to assumptions used to show the applicability of FRBs to cosmological tests, both the dispersion measure and its standard deviation calculated for host galaxies with given stellar mass in general increase with the redshift. The effect is not strong and cosmological tests using FRBs will be possible, but to preserve the level of statistical uncertainty the number of FRBs with known redshift in a sample should be increased by 15%–35% depending on circumstances. We show various statistical characteristics of ionized gas surrounding galaxies, the resulting dispersion measure and their dependence on the host galaxy stellar mass, redshift, and the projected distance of a FRB source from its host center.

**Key words:** *Cosmology: theory – Galaxies: halos – large-scale structure of Universe*

**1. Introduction**

Fast radio bursts (FRB) (Lorimer *et al.* 2007) are short events of  $\approx 1$  ms duration observed at  $\approx 1$  GHz radio frequencies. They are astrophysical phenomena of as yet unknown origin (see the review by Cordes and Chatterjee 2019 – CC19, and references therein). The number of known FRBs exceeds one hundred\*, and it is likely to grow substantially in the near future.

The propagation effects related to FRB allow in principle estimating the dispersion measure ( $DM = \int n_e ds$ ), the rotation measure ( $RM = \int n_e B_{\parallel} ds$ ), and the emission measure ( $EM = \int n_e^2 ds$ ) which influence the delay of the arrival time  $\tau$  of the signal at low frequencies relative to high frequencies in proportion to  $\nu^{-2}$ ,  $\nu^{-3}$ , and  $\nu^{-4}$ . The integrals are along the propagation path,  $s$  measures the distance,  $n_e$  is the concentration of free electrons, and  $B_{\parallel}$  is the magnetic field component along the ray. The term proportional to  $\nu^{-2}$  is the easiest to measure and allows finding

---

\* <http://frbcatalog.org>

DM (Thornton *et al.* 2013). The rotation measure (RM) and the emission measure based on optical observations may be found in some cases (*e.g.*, in FRB 190608, Chittidi *et al.* 2020).

At high Galactic latitudes DM for FRBs is systematically higher than for pulsars (Thornton *et al.* 2013, CC19), which suggests their extra-Galactic origin. This, in turn, enables some cosmological tests using FRBs (*cf.* Gao, Li and Zhang 2014, Zhou *et al.* 2014, Lorimer 2016, Yu and Wang 2017, Walters *et al.* 2018). To use FRBs in cosmological tests one needs the redshifts of the sources, which cannot be measured using radio data alone and is done by finding a so called host galaxy of the source, where the burst was localized.

The localizations of the FRB sources, based on their positions on the sky and proximity to possible host galaxies, are reliably known in  $\approx 10$  cases. Macquart *et al.* (2020) report localizations of four bursts discovered by them and note another five localized by other authors – see the references therein. The host galaxies are of different morphological types. The sample of five bursts used by Macquart *et al.* (2020) in their analysis of the baryon content of the Universe have redshifts in the range of 0.118–0.522. The sources lie at the projected distances of 1.5–7.0 kpc from centers of their host galaxies.

The proposed cosmological tests using FRBs are mostly based on the redshift–dispersion measure relation for the cosmological part of the dispersion measure ( $DM_{\text{cosm}}(z)$ ). The observed  $DM_{\text{obs}}$  includes also other parts (Deng and Zhang 2014):

$$DM_{\text{obs}} = DM_{\text{MW}} + DM_{\text{cosm}} + DM_{\text{host}}/(1+z) + DM_{\text{source}}/(1+z) \quad (1)$$

where  $DM_{\text{MW}}$  is the contribution from the Milky Way,  $DM_{\text{cosm}}$  is due to the Inter Galactic Medium (IGM) and possible intervening halos of galaxies close to the line-of-sight,  $DM_{\text{host}}$  represents its locally measured value due to the ionized gas in the host galaxy, and  $DM_{\text{source}}$  (again in the source frame) represents the impact of the source immediate environment, which may contain dense plasma, as suggested by some theoretical models (*e.g.*, Metzger *et al.* 2019).  $DM_{\text{MW}}$  is usually assumed to be easy to estimate based on the map of Galactic pulsars dispersion measure, but may also contain some unknown part related to the Galaxy halo (Prochaska and Zheng 2019).  $DM_{\text{source}}$  can be estimated based on the optical observations of the source environment and rotation measure of the burst as in the case of FRB 190608 (Chittidi *et al.* 2020).  $DM_{\text{host}}$  (which excludes the source vicinity) can be estimated only statistically, based on the host properties and the location of the source relative to the host center.

In a conservative approach to the cosmological tests based on FRBs (*e.g.*, Yang and Zhang 2016, Walters *et al.* 2018, Jaroszynski 2019, hereafter J19) it is assumed that the host contribution to the dispersion measure has a normal distribution which does not depend on time with the expected value  $\langle DM_{\text{host}} \rangle \approx 200 \text{ pc/cm}^3$  and the standard deviation  $\sigma_{\text{host}} \approx 50 \text{ pc/cm}^3$  (other values were also considered). Since

the expected value of the cosmological part increases with the redshift (approximately as  $DM_{\text{cosm}} \propto z$  – cf. Zhang 2018) and the contributions from hosts are divided by the  $1+z$  factor, their importance diminishes for far away sources, which makes cosmological tests plausible with a relatively small samples of FRBs with measured redshifts. Different properties of  $DM_{\text{host}}$  may require much bigger samples of the bursts for the tests.

In this article we investigate the contribution of the halos of galaxies to the observed dispersion measure using the results of IllustrisTNG-100 simulation (Nelson *et al.* 2018). In the next section we describe our method of finding the angle averaged distribution of free electrons as a function of the distance from the center of a galaxy. In Section 3 we calculate the dispersion measure for hosts of various stellar masses at the redshifts  $0 \leq z \leq 3$ . We give the results averaged over all possible locations of a source inside a galaxy and also for sources at a given projected distance from the galaxy center. The discussion follows in the last section.

## 2. Distribution of Free Electrons around Galaxies

The IllustrisTNG-100 simulation (Nelson *et al.* 2018, Pillepich *et al.* 2018, Springel *et al.* 2018, Naiman *et al.* 2018, Marinacci *et al.* 2018) gives the distribution of gas and gravitationally bound halos in a simulation cube of the size of  $75/h$  Mpc. Positions of the halos, dark matter particles, and gas cells, their masses, and other relevant parameters are accessible from IllustrisTNG database (Nelson *et al.* 2019). Some of the dense gas cells may become wind particles and possibly stars according to Illustris naming convention. They are treated separately and constitute a dedicated part of the database. If the star formation has already taken place, star particles have assigned luminosities in several filters. This gives the opportunity to distinguish galaxies from dark halos: we treat an object as a galaxy if it consists of a halo with star particles within 30 kpc from its center. The diffuse gas is present in the vicinities of so defined galaxies and around dark halos as well. Assuming that FRBs are somehow related to stars and products of their evolution, we limit ourselves to investigate galaxies.

Because of the technical limitations (data volume) we are able to use the lowest resolution version of the full cube simulation named TNG100-3. (Compare J19, based on Illustris-3 data for the same reason). Some numerical experiments with TNG100-3 show that the number of star cells within  $\approx 10$  kpc around galaxy centers is too small to give realistic maps of their distribution there, even if we stack distributions around many galaxies. For this reason we also use data from the simulations limited to smaller volumes but having better spatial resolution named TNG100-1-Subbox0 and TNG100-1-Subbox1. We consider several of the snapshots corresponding to the redshifts  $z = 0, 0.2, 0.5, 0.7, 1.0, 2.0$ , and  $3.0$  which should give a representative description of changes in gas and stars distribution with time.

For the subboxes the information on the gravitationally bound halos is not provided. We construct low resolution ( $1024^3$ ) 3D maps of total matter density within subboxes and look for its local maxima. For each maximum we investigate radial density distribution in its vicinity by counting mass in thin spherical shells. We proceed until the averaged density within the sphere falls to  $\approx 200\rho_c$ ,  $\rho_c$  being the critical matter density calculated for the given epoch. Next we find the sphere containing half of the total mass. For the matter inside this sphere we calculate its center of mass and repeat the calculation of radial mass distribution around it. After a few iterations we obtain a galaxy candidate with a given center of mass position. It may happen that our algorithm, starting from different local mass density maxima produces at the end more than one galaxy candidate at the same or very close positions. We remove these extra candidates if necessary. We also remove candidates which have no stars and constitute dark halos. When looking for the candidate galaxies we establish characteristics of their different component distributions:  $r_*$  – half star radius (of a sphere containing half of the star mass), and similarly  $r_{\text{gas}}$  for gas, and  $r_{\text{dark}}$  for dark particles. (Same parameters are provided for the halos in IllustrisTNG-100-3 database.)

Our goal is to estimate the distribution of the dispersion measure related to the host galaxy for a source randomly located inside it. In a brute force approach one would consider many source positions inside each galaxy and many paths going from a source to infinity checking the gas cells on the way and including their individual contributions to the dispersion measure. Such an approach is technically challenging (what is the contribution to the dispersion measure of a given gas cell if a ray passes at a given distance from its center?) and not necessary to obtain results averaged over many source positions and many ray directions. We assume that the location of sources follows the distribution of stars. The direction of the line-of-sight relative to the host galaxy for a given source location depends on the observer position. Isotropy of the Universe implies isotropic distribution of observers relative to the source and isotropic distribution of their lines-of-sight. Going a step further we also assume that (if averaged over many host galaxies) the distribution of stars and gas is spherically symmetric relative to the galaxy mass center. Under such simplifying assumptions it is only necessary to consider sources at different distances from the host center and rays making different angles with the direction toward the center, so the parameter space which should be investigated is two-dimensional.

We expect some dependence of DM on the host properties. Such relation should include parameters which can be measured to be useful. We have considered the total mass of stars and luminosities in different filters, which can be estimated with photometric observations. Since Illustris database provides masses of the stellar cells and their absolute luminosities in several filters, the synthetic galaxy parameters can be calculated. We found the total stellar mass to be the most convenient parameter. We divide all galaxies into seven bins with equal logarithmic

mic widths (0.5 dex) covering the range  $7.5 \leq \lg M_* \leq 11.0$  where  $M_*$  is the total stellar mass in solar units. We also put an upper limit on the total galaxy mass  $M_{\text{tot}} \leq 10^{13} M_\odot$  to exclude galaxy clusters and groups, which are systems of different kind.

We construct gas distributions stacking galaxies belonging to different mass ranges separately. We are interested in electron density  $n_e$  as a function of the distance from the galaxy center  $r$ . Our grid covers the radii from 1 kpc to 10 Mpc with equal logarithmic bins (0.1 dex). For each galaxy we consider gas cells within  $2r_{\text{gas}}$ . The number of free electrons in a gas cell is given by parameters from the database:

$$N_e = A \frac{X M_{\text{gas}}}{m_H} \quad (2)$$

where  $A$  is the ratio of the electrons number to the hydrogen atoms number inside the cell,  $M_{\text{gas}}$  is the total gas mass, and  $m_H$  is the hydrogen atom mass. In calculations we use the hydrogen mass fraction  $X = 0.75$ . The volume of the gas cell  $V$  is also given in the database, so the mean electron concentration  $n_e = N_e/V$  can be calculated. For further use we divide the interesting range of the comoving electron densities (from  $10^{-10}$  to  $10^0 \text{ cm}^{-3}$ ) into a hundred equal logarithmic bins. Electron concentration of each cell belongs to one of these bins.

At the starting point of the simulation gas cells have typical comoving sizes of  $75\,000/1820 h^{-1} \approx 41 h^{-1}$  kpc, much more than the thickness of the spherical shells in our radial grid close to the center. Gas cells which happen to be close to the center of a galaxy are much smaller and denser than the average but some of them would not fit into a single shell. We assign a gas cell to a radial bin if its center coordinates fall within. Redistribution of gas into adjacent radial bins is not possible since the shape of the cells is not given. (Assuming spherical shape leads to rather unpleasant calculations which are not worth the effort.) Instead we consider the averaged electron density in all cells whose centers fall into a given radial bin around a galaxy belonging to a given mass bin. We construct a histogram  $\text{Vol}(r^i, M_*^j, n_e^k)$ . If the center of a gas cell of volume  $V$  lies in the  $i$ -th radial bin surrounding a galaxy belonging to the  $j$ -th mass bin and has electron concentration belonging to the  $k$ -th density bin, the histogram changes according to the rule:

$$\text{Vol}(r^i, M_*^j, n_e^k) \rightarrow \text{Vol}(r^i, M_*^j, n_e^k) + V. \quad (3)$$

After checking positions of all gas cells relative to all galaxy centers we calculate the averaged electron densities:

$$\langle n_e(r^i, M_*^j) \rangle = \frac{\sum_k n_e^k \text{Vol}(r^i, M_*^j, n_e^k)}{\sum_k \text{Vol}(r^i, M_*^j, n_e^k)}. \quad (4)$$

Since all gas cells fill the whole simulation cube to a good approximation, the density defined above is realistic: there is no empty space around the cells which would increase the denominator and the cells do not overlap.

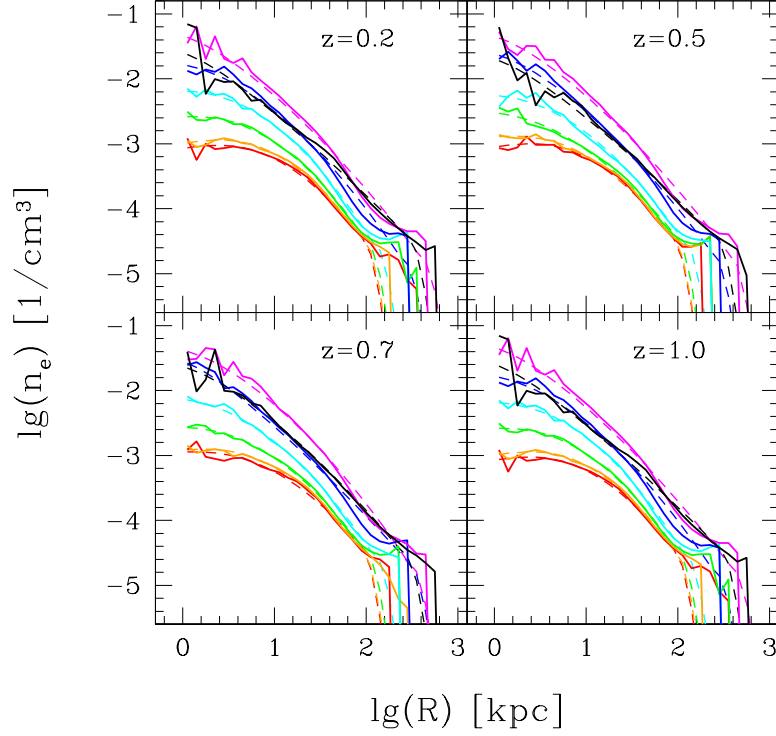


Fig. 1. Electron concentration profiles in galaxies belonging to different stellar mass ranges at different redshifts (solid lines). The redshifts are given by the labels and the mass ranges by colors:  $\lg(M_*/M_\odot) \in [7.5, 8.0]$  (red),  $[8.0, 8.5]$  (orange),  $[8.5, 9.0]$  (green),  $[9.0, 9.5]$  (cyan),  $[9.5, 10.0]$  (blue),  $[10.0, 10.5]$  (magenta), and  $[10.5, 11.0]$  (black). The plots for bins 1–6 are ordered and drawn with colors. The plots for the highest mass bin cross the other and we use black color to draw them. The rough analytical approximations to the density profiles are marked with dashed lines. (See text for details.) We use comoving distances and comoving densities; the true distances are smaller by a  $(1+z)$  factor, and the densities are  $(1+z)^3$  times higher.

The electron density profiles for several redshifts and galaxy mass bins are shown in Fig. 1. Due to the binning of the data and relatively small number of gas cells close to the center, the result is not a smooth function of  $r$ . It represents a typical dependence on the radius at a discrete set of points for a halo belonging to one of the considered mass ranges. The electron density profiles for  $M_* \leq 3 \times 10^{10} M_\odot$  are ordered, *i.e.*, the density increases with mass for a fixed radius. The highest mass range is exceptional: its density plot crosses the plots for the lower mass ranges. At  $z = 3$  the effect is absent. Relatively lower density of the electrons close to the centers of high mass galaxies implies their lower dispersion measure (see Section 3).

For further application we find a rough analytical approximation to the electron concentration dependence on radius. We look for a fit of the form:

$$y(x) = a_0 + a_1 x + a_2 x^2 \quad \text{where} \quad x \equiv \lg r \quad \text{and} \quad y \equiv \lg n_e \quad (5)$$

where  $a_0$ ,  $a_1$ , and  $a_2$  are the fit parameters different for each mass bin.

In our approach only gas cells within  $2r_{\text{gas}}$  from a galaxy center are considered as belonging to it. Even within the single mass bin this parameter has some scatter. On the other hand the fiducial mass density  $200\rho_{\text{crit}}$  calculated for the given epoch, may serve as a typical density at the halo boundary. At the present epoch it corresponds to the electron concentration  $n_{e0} \approx 4 \times 10^{-5} \text{ cm}^{-3}$  (for baryon density parameter  $\Omega_B = 0.05$  and  $h = 0.7$ ). Inspecting the plots in Fig. 1 one can see that after reaching this density the concentration rapidly falls off. For  $x \geq x_{4.4}$ , where  $y(x_{4.4}) = -4.4 = \lg(4 \times 10^{-5})$ , we use an *ad hoc* approximation  $y(x) = -4.4 - 20(x - x_{4.4})^2$  which represents a cut-off. The original and approximated curves can be compared in Fig. 1.

### 3. Estimates of the Host Galaxy Contribution to the Dispersion Measure

Using the analytical approximation to the electron concentration profile  $n_e(r)$  as defined in Eqs. 4 and 5 for a given galaxy mass range one can calculate the dispersion measure along a line-of-sight. We define:

$$\text{DM}(R, s_0) = \int_{s_0}^{\infty} n_e(\sqrt{R^2 + s^2}) ds \quad (6)$$

where the line-of-sight is passing at the distance  $R$  from the galaxy center. The length along the line-of-sight is measured by  $s$  with  $s = 0$  at the closest point to the center.  $s_0$  defines the source position and the integration formally goes to infinity, but in practice electron density falls to zero at some radius (*cf.* Fig. 1) characteristic for each mass range.

For a source at the distance  $r$  from the halo center and a line-of-sight at the angle  $\theta$  relative to the direction toward the center one has:

$$\text{DM}_{\text{host}}(r, \theta) = \text{DM}(r \sin \theta, -r \cos \theta). \quad (7)$$

Perhaps some selection mechanism makes the sources in the far away or close part of the host more/less likely to be observed but having no data we assume that they are distributed with spherical symmetry, which implies uniform distribution of  $\mu = \cos \theta$  in the range  $(-1, +1)$ . The radial distribution of sources is also unknown. We use a very simplified approach assuming that the sources follow the mass distribution of stars.

Stellar cells have densities  $\approx 10^6$  times higher than average so there is no problem with their excessive sizes as compared to the thickness of radial bins in our grid. We construct histograms giving the distribution of stellar mass inside galaxies belonging to given mass bin,  $\text{Mass}(r^i, M_*^j)$  and the number of galaxies in each mass bin  $\text{Num}(M_*^j)$ . For a stellar cell of mass  $M$  in a distance belonging to the  $i$ -th radial bin surrounding a galaxy belonging to the  $j$ -th mass bin the histograms change according to:

$$\text{Mass}(r^i, M_*^j) \rightarrow \text{Mass}(r^i, M_*^j) + M \quad (8)$$

$$\text{Num}(M_*^j) \rightarrow \text{Num}(M_*^j) + 1 \quad (9)$$

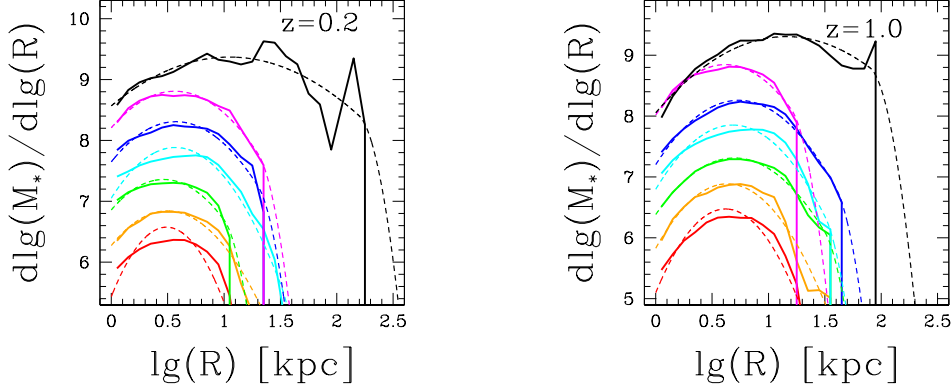


Fig. 2. Examples of the stellar mass distribution in galaxies belonging to different mass ranges for  $z = 0.2$  and  $z = 1.0$  as labeled. Color conventions follow Fig. 1. The raw data are plotted with solid lines and the analytical approximation uses dashed lines. See text for details.

After checking positions of all stellar cells relative to all galaxy centers we obtain the averaged stellar mass in a radial bin surrounding a galaxy belonging to given mass bin:

$$M^j(r^i) = \frac{\text{Mass}(r^i, M_*^j)}{\text{Num}(M_*^j)}. \quad (10)$$

In our approach the mass of stars in a spherical shell around a galaxy center is a relevant variable giving the relative probability of finding a source within the same radius range. In Fig. 2 we show the distribution of star mass in spherical shells of the same logarithmic thickness (0.1 dex) around galaxies of different mass ranges based on IllustrisTNG results for chosen epochs. The volumes of considered shells  $V(r) \propto r^3$ , so the mass distributions have maxima at a few kiloparsecs from the center, despite the fact that the averaged density of stars is a monotonically decreasing function of radius. Our analytic approximations (see Fig. 2) are obtained with a method very similar to the method applied to the electron density profiles. Using the approximated radial star mass distribution  $M^j(r)$  we have the approximated star density:

$$\rho_*^j(r) = \frac{dM^j/dr}{4\pi r^2}. \quad (11)$$

For each galaxy mass range we calculate DM on a grid of source positions distributed uniformly in  $\lg r$  and  $\mu$ . Under our assumption the probability  $p(\lg r, \mu)$  of finding a source position at any point of the grid scales as  $p(\lg r, \mu) \propto dM_*/d\lg r$ . After calculating DM along many paths we obtain its probability distributions separately for each galaxy mass range. These are distributions resulting from averaging over all possible source positions. They are shown in Fig. 3. To make the plots readable we transform the density probability functions  $f^j(DM)$  to have  $\max(f^j(DM)) = 1$ , where the subscript  $j$  enumerates the mass bins. The averaged



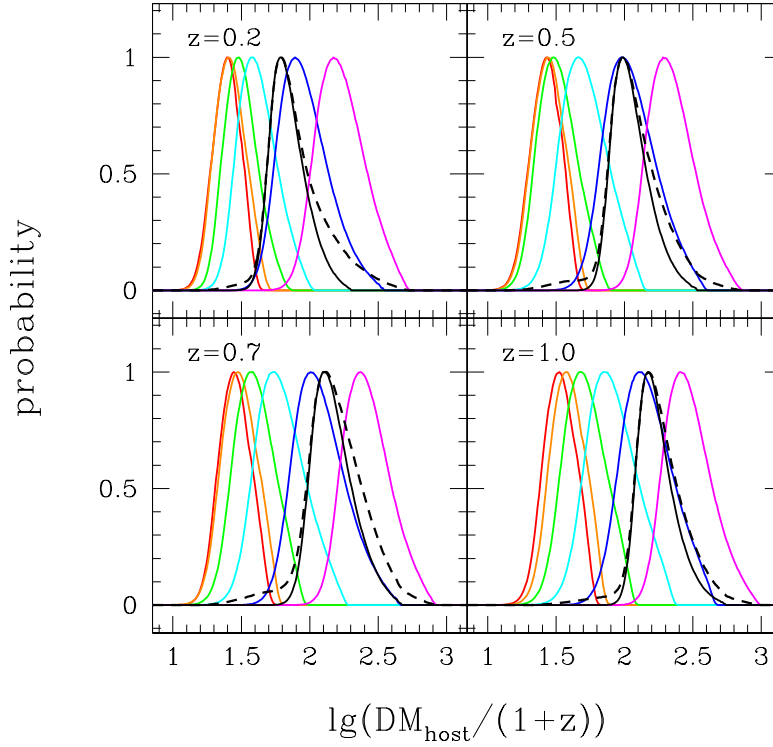


Fig. 3. Distributions of probability for the host galaxy contribution to the dispersion measure (DM), normalized to one at maximum. The color convention follows previous figures. The distribution averaged over seven mass bins is plotted as black dashed line. Panels correspond to different redshifts as denoted by labels. DM-s are calculated in the rest frames of the sources and divided by the  $1+z$  factor to represent their contribution to the total observed value.

$DM^j$  for given mass bin and its variance are given by standard expressions:

$$\langle DM^j \rangle = \frac{1}{A^j} \int_0^\infty DM f^j(DM) dDM \quad (12)$$

$$\sigma_{DM}^2 = \frac{1}{A^j} \int_0^\infty (DM - \langle DM^j \rangle)^2 f^j(DM) dDM \quad (13)$$

$$A^j = \int f^j(DM) dDM \quad (14)$$

where  $A^j$  is a normalizing factor. Finally we obtain the probability distribution for all the combined mass ranges. Denoting by  $M_*^j$  the total mass of stars in galaxies belonging to the  $j$ -th mass bin and by  $M_*^{\text{tot}}$  their sum, we have:

$$f(DM) = \sum_{j=1}^7 \frac{M_*^j}{M_*^{\text{tot}}} \frac{1}{A^j} f^j(DM) \quad (15)$$

In some cases the distance between the FRB's line-of-sight and the host center may be measured. This gives an extra constraint on the source position inside

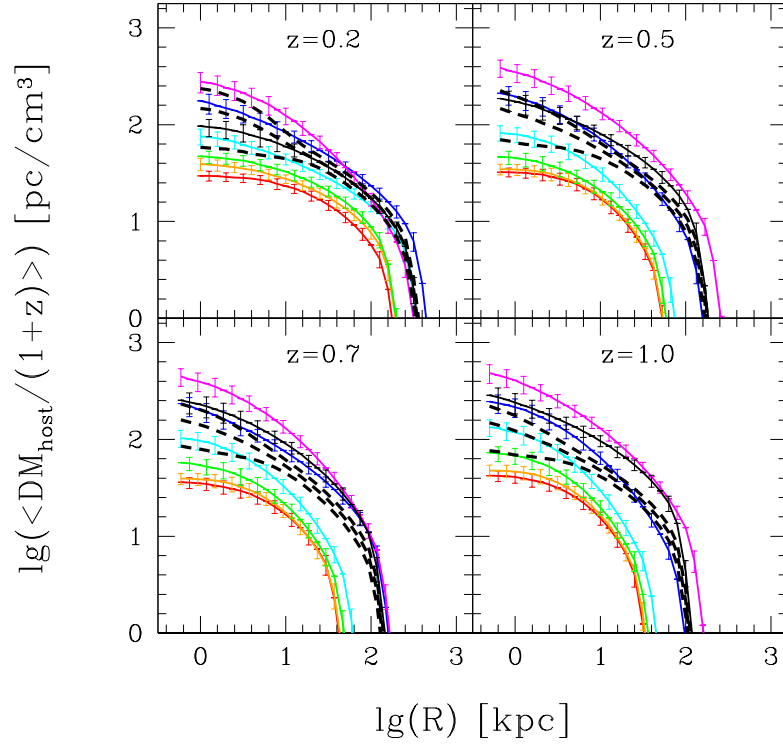


Fig. 4. The host galaxy contribution to the observed dispersion measure as a function of its physical distance from the line-of-sight. Color lines with error bars give the results for different galaxy mass ranges averaged over source positions along the line-of-sight. The color convention follows previous figures. Results for hosts at different redshifts are shown in separate panels, as labeled. The averages over all mass ranges and their  $\pm$  sigma deviations are shown using thick black dashed lines.

the host galaxy. Since we assume that the sources follow the distribution of stars and the density of stars decreases sharply with increasing distance from the host center, the vicinity of the point closest to the center on the line-of-sight is the most probable position of the source. For a line-of-sight passing at the distance  $R$  from the host center and the source at position  $s_0$  along the line-of-sight the dispersion measure  $DM(R, s_0)$  is given by Eq.(6). The probability of the source position  $s_0$  at given  $R$  is proportional to the star density  $\rho_*^j \left( \sqrt{R^2 + s_0^2} \right)$ , so the average dispersion measure and its variance for the  $j$ -th galaxy mass range are given by:

$$\langle DM^j(R) \rangle = \frac{1}{B^j} \int_{-\infty}^{+\infty} DM^j(R, s_0) \rho_*^j \left( \sqrt{R^2 + s_0^2} \right) ds_0 \quad (16)$$

$$\sigma_{DM}^2 = \frac{1}{B^j} \int_{-\infty}^{+\infty} (DM^j(R, s_0) - \langle DM^j(R) \rangle)^2 \rho_*^j \left( \sqrt{R^2 + s_0^2} \right) ds_0 \quad (17)$$

$$B^j = \text{Num}(M_*^j) \int_{-\infty}^{+\infty} \rho_*^j \left( \sqrt{R^2 + s_0^2} \right) ds_0 \quad (18)$$

where  $B^j$  is a normalizing factor. The averaged over all mass ranges  $\langle \text{DM}(R) \rangle$  can be obtained as weighted mean of  $\langle \text{DM}^j(R) \rangle$  with weights proportional to  $B^j$ .

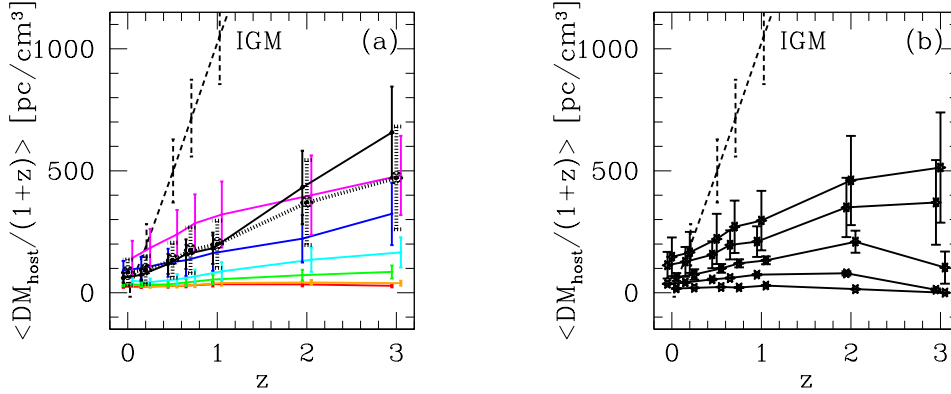


Fig. 5. (a) The source position averaged contribution of the host galaxy to the observed dispersion measure  $\text{DM}_{\text{host}}/(1+z)$  and its standard deviation  $\sigma_{\text{host}}/(1+z)$  (error bars) as a function of the redshift for different mass ranges (color conventions follow Fig. 1). The thick solid line with asterisks gives the dependence averaged over the whole host mass range. (b) The host contribution to the observed dispersion measure averaged over all mass ranges and source position along the line-of-sight at given physical distance from the galaxy center: 0 kpc, 3 kpc, 10 kpc, 30 kpc, and 100 kpc (top to bottom) with standard deviation (error bars) as a function of the redshift. In *both panels* the positions of the error bars are slightly shifted in redshift to avoid their overlapping. The dashed lines show the cumulative dispersion measure and its standard deviation due to the IGM between the observer and given redshift, based on the data from J19.

The averaged dispersion measures for all host mass bins as a function of the projected distance from the host center  $R$  are given in Fig. 4 with standard deviations shown as error bars. In Fig. 5a we show dispersion measures DM and their standard deviations  $\sigma_{\text{DM}}$  as a function of the redshift for different galaxy mass ranges, averaged over all possible source positions. In Fig. 5b we show DM and its standard deviation as a function of the redshift for sources at known projected distances from the galaxy center, averaged over all galaxy mass ranges.

We also present our numerical results in Table 1. The table gives the contributions to the observed dispersion measure as a function of the redshift (1-st column). For comparison in the 2-nd column we give the expected contribution from IGM, as calculated by J19. The 3-rd column ( $\langle \text{DM} \rangle$ ) gives the expected contribution averaged over galaxies of all mass ranges and all possible source positions assumed to follow the distribution of stars. The remaining five columns give the expected contribution  $\text{DM}_R$  for a source at projected distance  $R$  (where  $R = 0$  kpc, 3 kpc, 10 kpc, 30 kpc, and 100 kpc respectively) from a galaxy center, averaged over all galaxy mass ranges.

Our calculations show that in general the contribution of the hosts to the observed dispersion measure increases with the redshift despite the  $1/(1+z)$  reducing factor. This can be seen in Fig. 5a for galaxy mass ranges with  $M_* \geq$

$3 \times 10^8 M_\odot$ . It is also true about the standard deviations, which may reach values of  $100\text{--}200 \text{ pc/cm}^3$  at source redshifts  $1 \leq z \leq 3$ . On the other hand for galaxies with small masses  $M_* \leq 3 \times 10^8 M_\odot$  (two low mass ranges) DM and  $\sigma_{\text{DM}}$  remain low.

Examining column  $\text{DM}_0$  in Table 1 one can see large values of DM and  $\sigma_{\text{DM}}$ , but this is an extreme case with a source in projection at the very center of the host, which has a low probability. At  $R \geq 30 \text{ kpc}$  the contribution from the hosts becomes negligible as compared to the expected IGM values for  $z \geq 0.5$ .

Table 1

Averaged host DM

$z$	$\text{DM}_{\text{IGM}}$	$\langle \text{DM} \rangle$	$\text{DM}_0$	$\text{DM}_3$	$\text{DM}_{10}$	$\text{DM}_{30}$	$\text{DM}_{100}$
0.0	$0 \pm 0$	$83 \pm 53$	$147 \pm 80$	$113 \pm 54$	$65 \pm 16$	$37 \pm 1$	$17 \pm 0$
0.2	$187 \pm 85$	$93 \pm 58$	$165 \pm 84$	$127 \pm 61$	$75 \pm 22$	$42 \pm 2$	$20 \pm 0$
0.5	$493 \pm 129$	$133 \pm 72$	$221 \pm 103$	$156 \pm 55$	$100 \pm 18$	$55 \pm 3$	$23 \pm 0$
0.7	$705 \pm 157$	$174 \pm 93$	$271 \pm 108$	$196 \pm 60$	$120 \pm 17$	$60 \pm 2$	$21 \pm 0$
1.0	$1025 \pm 197$	$198 \pm 97$	$296 \pm 122$	$210 \pm 63$	$133 \pm 16$	$74 \pm 2$	$30 \pm 0$
2.0	$2045 \pm 293$	$370 \pm 174$	$460 \pm 183$	$350 \pm 121$	$209 \pm 45$	$80 \pm 9$	$15 \pm 1$
3.0	$2968 \pm 345$	$471 \pm 210$	$513 \pm 226$	$370 \pm 174$	$103 \pm 66$	$12 \pm 6$	$1 \pm 0$

#### 4. Discussion

Our results do not support the standard assumptions used when investigating the plausibility of cosmological tests based on FRBs with known redshifts. As we have shown the contribution from the host galaxy to the dispersion measure is in general an increasing function of the redshift and its standard deviation follows similar path, which contradicts the hypothesis that both quantities decrease in proportion to  $1/(1+z)$ . This is not a fundamental problem, but makes the tests more difficult, since for a given accuracy one needs larger samples of FRBs with measured redshifts.

Due to the inhomogeneity of the IGM its expected dispersion measure  $\text{DM}_{\text{IGM}}(z)$  has some scatter  $\sigma_{\text{IGM}}(z)$  (compare Table 1, column 2). The scatter in the host contribution  $\sigma_h(z) \equiv \sigma_{\text{host}}/(1+z)$  (given in the remaining columns) increases the statistical noise. The combined variance of the IGM and the host contributions,  $(\sigma_{\text{IGM}}^2(z) + \sigma_h^2(z))$ , should be compared with the variance of the IGM part alone ( $\sigma_{\text{IGM}}^2(z)$ ). Taking  $\sigma_h$  values from the 3-rd column of Table 1 we see increase of 31% at  $z = 0.5$ , and 37% at  $z = 3$ . Similarly, for the 5-th column (source at 3 kpc from the host center) we obtain 18% and 25% respectively. To preserve the postulated statistical accuracy of the cosmological tests the number of FRBs in a sample should increase in proportion. Since this increase is moderate, the simulations of

the accuracy of cosmological tests based on FRBs under conservative assumptions remain valid.

Our predictions of the host contribution to  $DM_{\text{obs}}$  as shown in Figs. 3–5 may give some guidance when considering real objects. One can see that the contribution from galaxies with low stellar mass  $M_* \leq 10^9 M_\odot$  is practically unimportant, but it is also unlikely that they are recognized as hosts at cosmologically interesting redshifts due to their low luminosity. Looking at the galaxy mass averaged results one can see that at the projected distance  $R \geq 30$  kpc at  $z \geq 0.5$  the hosts contribution becomes much smaller than the IGM value or its standard deviation.

Prochaska and Zheng (2019) estimate the dispersion measure of our Galaxy halo as observed from the Sun position to be  $50\text{--}80 \text{ pc/cm}^3$ . Their analysis is based on observations of O VI and O VII ions which trace the ionized hydrogen. The stellar mass of the Milky Way  $M_* \approx 6 \times 10^{10} M_\odot$  (Licquia and Newman 2015) places it in the highest mass bin considered here. Our results for a line-of-sight at 8 kpc from a galaxy belonging to the highest mass bin at  $z = 0$  give  $DM_{\text{host}} = 64 \pm 12 \text{ pc/cm}^3$  in an excellent agreement with the value quoted above.

Chittidi *et al.* (2020) estimate the dispersion measure of the halo of (as they call it) HG 190608 galaxy, which is the host of FRB 190608, at  $z = 0.12$ . The galaxy has stellar mass  $M_* = 2.5 \times 10^{10} M_\odot$  and the source position is at  $R = 8$  kpc from the center. Following the methods of Prochaska and Zheng (2019) the authors estimate the halo contribution to DM to be in the limits of  $30\text{--}80 \text{ pc/cm}^3$ . The galaxy stellar mass places it in the second highest mass range considered here and close to the boundary with the highest mass range. Using our results for the  $10^{10} \leq M_* \leq 3 \times 10^{10} M_\odot$  and interpolating between redshifts we obtain  $DM_{\text{host}}/(1+z) = 144 \pm 30 \text{ pc/cm}^3$ , about three times higher estimate. Using the results for the highest mass range we would have  $67 \pm 12$  (same units) and interpolating in mass and redshift  $115 \pm 23$ . Thus our prediction of the HG 190608 halo contribution to the observed DM is one to three times higher as compared to the work of Chittidi *et al.* (2020) depending on methodology.

Bhandari *et al.* (2020) examine various properties of the four host galaxies localized with the Australian SKA Pathfinder telescope. These galaxies have  $\lg(M_*/M_\odot) \approx 9.4\text{--}10.4$ , and the redshifts  $0.11 \leq z \leq 0.48$ . Using our results for  $z = 0.2$  one would predict their halo contributions to DM to be (depending on mass)  $44 \pm 15$  to  $184 \pm 78 \text{ [pc/cm}^3]$ . Macquart *et al.* (2020) uses a sample of five FRBs (including four mentioned above) to estimate the density of baryons in the Universe based on the observed DM. The host contribution is modeled statistically: it is assumed that  $DM_{\text{host}}$  has log-normal distribution. The four parameter model is fitted to the data and gives a weak constraint on hosts:  $\langle DM_{\text{host}} \rangle \approx 100$  and  $50 \leq DM_{\text{host}} \leq 200 \text{ [pc/cm}^3]$ , which agrees well with our estimates.

The hosts contribution to the observed DM is a technical problem making cosmological applications of FRBs difficult. With the growing number of known bursts the correlations of the observed DM with the number and types of objects near

the line-of-sight may give some limits on  $DM_{\text{host}}$  (compare Prochaska and Zheng 2019). On the other hand detailed studies of particular hosts, like work performed by Chittidi *et al.* (2020) on HG 90608 should lead to more stringent relations allowing more accurate estimates of  $DM_{\text{host}}$  based on other host properties.

*Note added in proofs:*

After this article had been submitted, the work on the same subject, also based on IllustrisTNG simulation, but using different methods was published by Zhang *et al.* (2020).

**Acknowledgements.** The IllustrisTNG Simulation databases used in this paper and the web application providing on-line access to them were constructed as part of the activities of the German Astrophysical Virtual Observatory.

## REFERENCES

- Bhandari, S., *et al.* 2020, *ApJ*, **895**, L37.  
 Chittidi, J.S., *et al.* 2020, arXiv2005.13158.  
 Cordes, J.M., and Chatterjee, S. 2019, *Ann. Rev. Astron. Astrophys.*, **57**, 417 (CC19).  
 Deng, W., and Zhang, B. 2014, *ApJ*, **783**, L35.  
 Gao, H., Li, Z., and Zhang, B. 2014, *ApJ*, **788**, 189.  
 Jaroszynski, M. 2019, *MNRAS*, **484**, 1637 (J19).  
 Licquia, T.C., and Newman, J.A. 2015, *ApJ*, **806**, 96.  
 Lorimer, D. 2016, *Nature*, **530**, 427.  
 Lorimer, D.R., Bailes, M., McLaughlin, M.A., Narkevic, D.J., and Crawford, F. 2007, *Science*, **318**, 777.  
 Macquart, J.-P., *et al.* 2020, *Nature*, **581**, 391.  
 Marinacci, F., *et al.* 2018, *MNRAS*, **480**, 5113.  
 Metzger, B.D., Margalit, B., and Sironi, L. 2019, *MNRAS*, **485**, 4091.  
 Naiman, J.P., *et al.* 2018, *MNRAS*, **477**, 1206.  
 Nelson, D., *et al.* 2018, *MNRAS*, **475**, 624.  
 Nelson, D., *et al.* 2019, *Computational Astrophysics and Cosmology*, **6**, 2.  
 Pillepich, A., *et al.* 2018, *MNRAS*, **475**, 648.  
 Prochaska, J.X., and Zheng, Y. 2019, *MNRAS*, **485**, 648.  
 Springel, V., *et al.* 2018, *MNRAS*, **475**, 676.  
 Thornton, D., *et al.* 2013, *Science*, **341**, 53.  
 Yang, Y.-P., and Zhang, B. 2016, *ApJ*, **830**, L31.  
 Yu, H., and Wang, F.Y. 2017, *A&A*, **606**, 3.  
 Walters, A., Weltman, A., Gaensler, B.M., Ma, Y.-Z., and Witzemann, A. 2018, *ApJ*, **856**, 65.  
 Zhang, B. 2018, *ApJ*, **867**, L21.  
 Zhang, G.Q., Yu, H., He, J.H., and Wang, F.Y. 2020, arXiv:2007.13935.  
 Zhou, B., Li, X., Wang, T., Fan, Y.-Z., and Wei, D.-M. 2014, *Phys. Rev. D*, **89**, 107303.